Article

Controllable CaF$_2$ Nanosized Stripe Arrays on Si(001) Studied by X-ray and Electron Diffraction

Sergey M. Suturin [1,*] **, Vladimir V. Fedorov** [2] **, Alexander M. Korovin** [1] **, Gleb A. Valkovskiy** [3] **, Masao Tabuchi** [4] **and Nikolai S. Sokolov** [1]

1   Ioffe Institute, 26 Polytechnicheskaya, 194021 St. Petersburg, Russia; amkorovin@gmail.com (A.M.K.); nsokolov@fl.ioffe.ru (N.S.S.)
2   Laboratory of Renewable Energy Sources, Alferov University (formerly St. Petersburg Academic University), 194021 St. Petersburg, Russia; vfedorov.fl@mail.ioffe.ru
3   Faculty of Physics, St. Petersburg State University, 7-9 Universitetskaya nab., 199034 St. Petersburg, Russia; Valkovsky_Gleb@mail.ru
4   Synchrotron Radiation Research Center, Nagoya University, 464-8603 Nagoya, Japan; m.tabuchi@nusr.nagoya-u.ac.jp
*   Correspondence: suturin@mail.ioffe.ru

Abstract: Adding uniaxial in-plane anisotropy to the otherwise four-fold Si(001) surface has for a long time been known to be possible via epitaxial deposition of a single atomic layer of calcium fluoride (CaF$_2$), which forms an array of micron-long (110) oriented parallel stripes when the substrate temperature during the growth is kept in the range of 700–800 °C. As shown in the present paper, a fine control over dimensions and periodicity of the stripe array is possible through the introduction of a two-stage growth process at which the (110) orientation of the fluorite layer is settled at the high-temperature nucleation stage, while the stripes of controllable dimensions are formed at the second stage. By varying the substrate temperature at the second growth stage in the range of 800–400 °C, the stripe arrays with a periodicity from above 30 nm to below 10 nm can be fabricated with the height variation changing accordingly. Such variability can be of use in the applications in which the striped fluorite surface is used to influence the anisotropy of other functional (e.g., magnetically ordered or organic) materials grown on top. While large CaF$_2$ stripes can be easily characterized by direct space techniques such as atomic force microscopy, the study of the shape and in-plane correlation between the stripes of a much smaller size is most effectively achieved through the use of grazing incidence reciprocal space techniques applied in the present paper. The discussed universal approach to 3D reciprocal space mapping utilizing scattering of X-rays and high-energy electrons offers a complementary way to study samples with arrays of long and narrow one-dimensional stripes at their surface.

Keywords: calcium fluoride; 1D stripes; silicon; MBE; RHEED; XRD

1. Introduction

The choice of substrates for heteroepitaxial growth of functional heterostructures is usually limited to materials with good lattice matching and a possibility to prepare an atomically smooth substrate surface. The introduction of an intermediate buffer layer in between the substrate and the functional layer widens the choice of morphologies, symmetries and crystal structures of the surface to grow upon. For a long time, calcium fluoride (CaF$_2$) grown by molecular beam epitaxy on Si(111) has been considered a prototypical system for studying interfaces between materials with different kind of bonding [1–3] and a promising candidate for fabrication of multilayer structures for micro- and optoelectronics and as a buffer layer for III-V on Si integration [4,5]. The lattice matching is known to be reasonably good between calcium fluorite (a = 5.451 Å) and silicon (a = 5.431 Å). In our recent studies [6–11], CaF$_2$ buffer layers grown on Si have been used to investigate interface

magnetism at nanometer scale in ferroic-on-semiconductor systems with ferromagnetic Co and Ni nanoparticles and antiferromagnetic MnF_2 and NiF_2 layers. The main role of the non-magnetic CaF_2 buffer layer in these heterostructures was not only to prevent a chemical reaction between metal and silicon, but also to guide the nucleation of magnetically ordered structures with a given morphology and crystalline orientation. Specifically, the substrate-induced uniaxial magnetic anisotropy appears as the magnetic nanoparticles tend to form dense chains along the $CaF_2(111)$ atomic steps or $CaF_2(110)$ ridge tops. Another promising application is the use of self-organized regular ridge-and-valley $CaF_2(110)$ structures as templates for the graphoepitaxial growth of horizontal II-VI and III-V semiconductor nanowires on Si [12,13]. In Reference [14], Si quantum dot sheets were also grown on the epitaxial CaF_2 surface. Due to the high insulating properties of CaF_2 (ε = 8.43, Eg = 12.1 eV), this material has been also studied [15,16] as a promising alternative to amorphous oxides to be used in silicon-based field-effect transistors for which it can be grown by molecular-beam epitaxy [3]. Moreover, nanoscale MoS_2 field effect transistors with a record-thin 2 nm CaF_2 insulator layer have been recently demonstrated [17]. When grown on Si(111), calcium fluoride tends to form a uniform layer with an atomically flat (111) surface, whereas in a less widely studied CaF_2/Si(001) system discussed in the present paper, the growth follows a more exotic scenario. When epitaxially grown onto Si(001) surface, CaF_2 forms various types of 1D morphologies including nanowires and ridges [18,19], adding a two-fold local anisotropy to the otherwise 4-fold Si(001) surface. Although lattices of CaF_2 and Si are of similar fcc structure and well matched, during high-temperature growth, the CaF_2 lattice does not continue that of the substrate, showing the following complex epitaxial relations: $CaF_2(110)$ ∣∣ Si(001), $CaF_2(1-10)$ ∣∣ Si(1-10) [20]. Reflection high energy electron diffraction (RHEED), atomic force microscopy (AFM), X-ray photoemission and absorption spectroscopy were applied in a number of works [21,22] to investigate the growth modes of CaF_2 on Si(001), confirming that at a growth temperature of 700–770 °C a reacted monolayer consisting of rows of parallel nanostripes is formed at the silicon surface. The structural properties of this monolayer have been studied by scanning tunneling microscopy (STM) [23] and surface X-ray diffraction (SXRD) [24] to show that, at the initial stage, a certain degree of disorder and the related incommensurate structure appear at the surface. Ab initio calculations, based on pseudopotentials and density functional theory, were performed in Reference [25] to investigate the atomic geometry and electronic structures of calcium fluoride on the Si(001) surface. Structural, vibrational and electronic properties of single-layers and one-dimensional nanoribbons of CaF_2 were investigated using first-principle calculations in Reference [26]. The micron-long $CaF_2(110)$ sloped ridges forming at a higher fluorite coverage were successfully utilized in recent years as templates to produce ordered arrays of ferromagnetic nanoparticles [7–9,27] and to crystallographically align the magnetic anisotropy axis in antiferromagnetic MnF_2 and NiF_2. The fluorite gratings have been utilized as natural templates for aligning organic molecules. For example, in Reference [28], the ultra-thin semi-insulating layers of CaF_2/Si(100) were shown to orient hexaphenyl molecules adsorbed on top. Charge transfer dynamics in a single iron tetraphenylporphyrin donor/acceptor dyad adsorbed on a CaF_2/Si(100) insulating surface was investigated in References [29,30].

So far, the morphology of $CaF_2(110)$ stripes growing on the Si(001) surface has been studied mainly by atomic force microscopy, while electron diffraction has been used mainly to define epitaxial relations. In the present paper, we discuss crystal structure and surface morphology of the fluorite ridges on Si(001) by investigating the shape of diffuse scattering appearing around the CaF_2 Bragg reflections in X-ray diffraction (XRD) and reflection high energy electron diffraction (RHEED) as well as in the vicinity of reciprocal space origin in grazing-incidence small-angle X-ray scattering (GISAXS). This study has become possible with the recent introduction of the universal approach to 3D reciprocal space mapping by RHEED, XRD and GISAXS [9]. Analyzing not only the position of CaF_2 reciprocal space nodes but also the very peculiar diffuse scattering around them, we present an alternative

way to study the shape and in-plane correlation in the system of stripes, including those with a very small spacing that are difficult to investigate by AFM.

2. Materials and Methods

The fluorite layers were grown by molecular beam epitaxy onto low miscut silicon wafers of (001) orientation. The wafers were cleaned by Shiraki chemical treatment [31] prior to growth and flash-annealed to 1200 °C in ultra-high vacuum (UHV) to remove silicon oxide and to form an atomically flat step-and-terrace surface. Deposition of CaF_2 was performed in UHV conditions from an effusion cell at a rate of 2–3 nm/min. Crystallinity, epitaxial relations and defect structure were monitored by in situ high energy electron diffraction reciprocal space 3D mapping. Being a substantial improvement over the conventional RHEED, the reciprocal space mapping deals with a sequence of diffraction patterns taken while the sample is rocked [9,27]. A fine-step sequence of Ewald spherical sections obtained in this way is compiled into 3D intensity maps using the dedicated software [9]. The described approach allows demonstrating the reciprocal lattice structure in the easily interpreted form of planar cuts or projections along specific crystallographic directions. The XRD and GISAXS studies were carried out at BL3A beamline of Photon Factory synchrotron (Tsukuba, Japan) using photon energy of 12 keV. The 3D reciprocal space maps in both techniques were obtained with a PILATUS 100 K detector placed at 750 mm from the sample. Series of images were taken during fine-step azimuthal rotation of the sample placed onto the conventional four-circle Huber diffractometer. The obtained images were processed in the same way and using the same software as described above for RHEED. The wide-angle X-ray diffraction was carried out at 5 deg of incidence to increase surface sensitivity. GISAXS measurements were performed at 0.3–0.5 deg of incidence. Sample surface morphology was measured using NT-MDT atomic force microscope (AFM) operating at ambient air conditions.

3. Results and Discussion

As was shown in our recent publications [22], the lattice orientation of CaF_2 deposited onto Si(001) mimics the orientation of the substrate only when the growth is performed below 600 °C. At an elevated temperature of 700–800 °C, the growth proceeds along a less evident scenario. A dissociative reaction occurs at the surface, giving rise to the formation of a uniform wetting monoatomic layer of CaF bonded to silicon through Ca atoms [22]. This wetting layer changes the surface periodicity from double-domain 2×1 to single-domain 3×1. Further deposition of CaF_2 leads to the formation of elongated ridges or stripes on top of the wetting layer (Figure 1a). The CaF2[110] axis inside the ridge gets oriented perpendicular to the substrate and $CaF_2\{111\}$ slopes are formed on both sides of the ridge. The ridge can be considered a quasi 1D object as its length exceeds several microns, while its transverse dimensions remain in the tens-of-nm range.

Remarkably, the transverse dimension of the ridges can be effectively controlled by choosing the temperature at which CaF_2 is deposited on top of the already-formed wetting layer. Figure 1d–f show a series of AFM images taken on the samples in which the second stage CaF_2 deposition (total thickness 50–70 nm) was carried out at 800 °C, 620 °C and 440 °C. At 800 °C the ridges are 30 nm in size and the slopes on both sides of the ridge can be recognized. The samples grown at 620 °C and 440 °C exhibited similar AFM patterns with parallel stripes of 18 nm and 10 nm size, respectively. For low-T samples, the slopes cannot be easily recognized on the AFM images due to insufficient resolution related to the finite radius of the AFM tip. However, as will be shown later by RHEED, the slopes are present in all the samples. The temperature dependence of CaF_2 diffusion during the growth is the most likely reason for the observed behavior. For the more studied case of CaF_2 growth on Si(111), where the island nucleate and grow in an isotropic layer-by-layer manner, the characteristic size of the islands is known to reduce with temperature. For the $CaF_2(110)/Si(001)$ system, the growth occurs in a highly anisotropic way. The ridge growth in the longitudinal direction is almost unlimited, as there is an almost perfect lattice match

between CaF_2 and Si along the CaF2[1–10]/Si[1–10] axis. Quite opposite, the ridge growth in the transversal CaF2[001]/Si[110] direction is very limited and sharply dependent on the growth temperature. As shown in Reference [22], the wetting layer appearing at the very beginning of CaF_2 deposition consists of a densely packed array of nanostripes acting as nucleation sites for the further growth of the 3D fluorite ridges. The density of nucleation events will naturally increase as the diffusion length across the nanostripes gets smaller at a lower deposition temperature. Our RHEED studies confirm that once nucleated, the CaF_2 stripes grow with the same epitaxial relations of initially formed $CaF_2(110)$ wetting layer with respect to Si, independent of the substrate temperature at the second growth stage. The typical RHEED maps showing reciprocal space sections along and perpendicular to the stripes are shown in Figure 1b,c. The reciprocal space map with the [001] zone axis obtained with the e-beam perpendicular to the stripes (Figure 1c) shows a regular pattern of reciprocal space nodes corresponding to the CaF_2 lattice oriented with the [110] axis perpendicular to the surface. The slight elongation of the nodes perpendicular to the surface is associated with the flat areas between the ridges. The reciprocal space map with the [1–10] zone axis taken with the e-beam parallel to the stripes (Figure 1b) looks remarkably different, showing a pronounced net of inclined streaks and no well-defined reciprocal space nodes. The streaks are perpendicular to the side {111} facets of the ridges and are due to the small penetration depth of electrons traveling at a grazing incidence to these facets. An important prerequisite for such streaks to appear is the atomic smoothness of the facets.
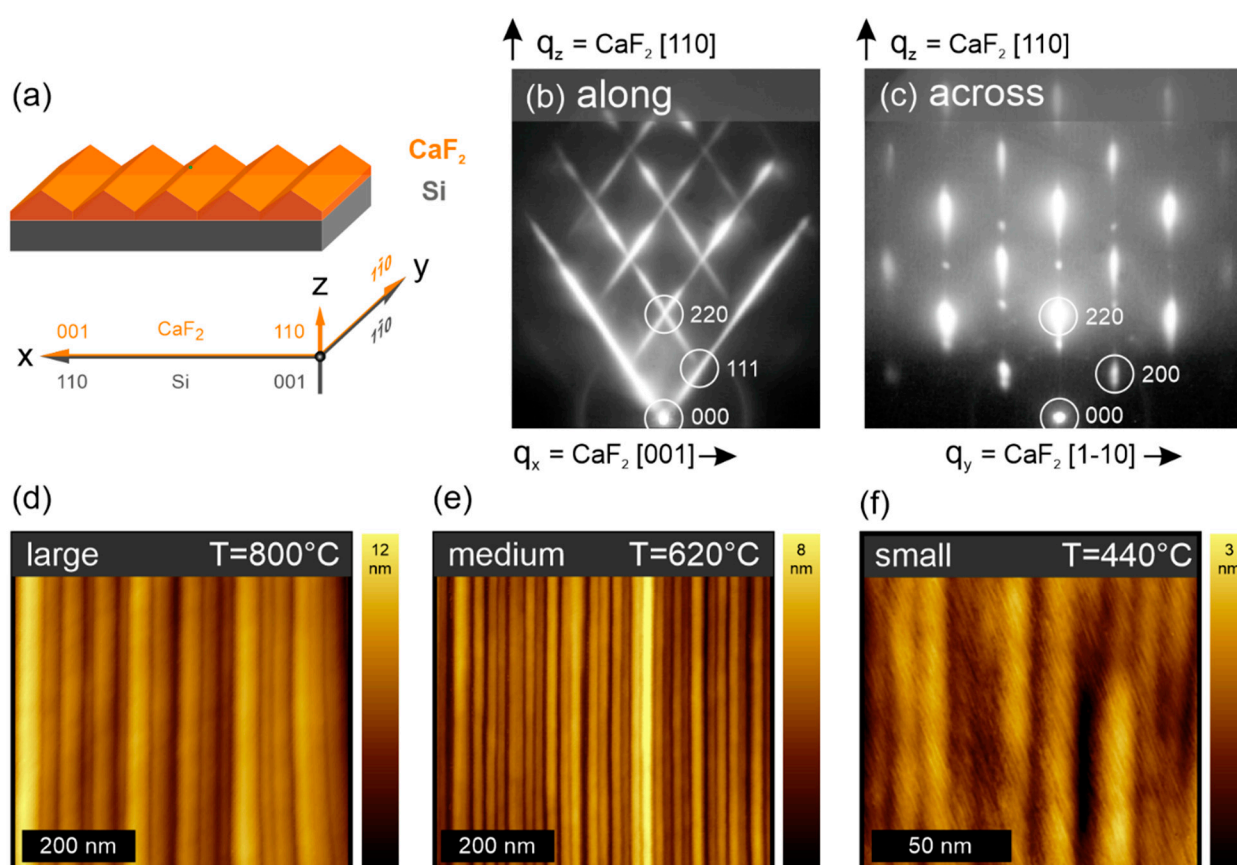

Figure 1. A schematic drawing of the fluorite ridge shaped stripes and the corresponding epitaxial relations between CaF_2 and Si (**a**). Reflection high energy electron diffraction (RHEED) reciprocal space maps obtained with the e-beam incident along (**b**) and across (**c**) the stripes. The inclined streaks correspond to the grazing incidence diffraction from the {111} side slopes of the ridge. A series of AFM images of CaF_2 stripes grown at 800 °C (**d**), 620 °C (**e**) and 440 °C (**f**). The corresponding inter-stripe periods are 33, 18 and 10 nm. Axis q_z is perpendicular to the substrate surface, axis q_x is perpendicular to the stripes.

Further structural investigation of the CaF$_2$ stripes on Si(001) was carried out by grazing-incidence small-angle X-ray scattering. With the X-ray beam aligned parallel to the stripe direction, the GISAXS pattern consists of an arc and a couple of vertical streaks to the left/right of the direct beam (Figure 2). Remarkably, the GISAXS patterns show an unusually sharp dependence on the azimuthal angle, which is the angle between the beam and the stripes. As shown in Figure 2d, the arc is symmetric at $\phi = 0$ deg but becomes very asymmetric at ϕ as small as 0.1 deg and disappears almost completely at angles larger than 1 deg. The intensity and position of the side streaks also change with the azimuthal angle so that the brightest part of the streak is the one located close to the arc. Such unusual behavior is specific to the scattering from 1D objects (which in our case extend to a micron size along the beam and are confined to nanometer size in the perpendicular direction). Similar arc-like GISAXS patterns have been reported previously by other research groups, e.g., for highly ordered gratings, fabricated on silicon by electron beam lithography or on polymer films by nanoimprint lithography [32]. In Reference [33], GISAXS was measured for a grating written with an e-beam on a quartz substrate and covered by a layer of ruthenium. Both these works deal with the gratings produced by the top-down approach and having a period in the range of hundreds of nanometers. The CaF$_2$/Si(001) gratings discussed in the present work differ in that they are self-assembled gratings, have a much smaller pitch of 10–30 nm and are less correlated, as will be shown below. The reason for which an arc is observed in GISAXS is that the Fourier transform of a 1D object is confined within a thin reciprocal space sheet oriented perpendicular to the stripe direction. The thickness of this sheet is inversely proportional to the length of the 1D object, which is in the micron range. Thus, for a wavelength of 1 Å, the sheet thickness is about 10,000 times smaller than the Ewald sphere radius. For this reason, a single GISAXS pattern, which is an intersection of the reciprocal space sheet with the Ewald sphere allows imaging only a very small arc-like portion of the reciprocal space sheet (Figure 2a). As the sample is rotated azimuthally, the Ewald sphere intersects different parts of the reciprocal space sheet, and the arcs move accordingly. In order to image intensity in the q_{xz} plane, we have acquired a sequence of GISAXS images, while the sample was rotated azimuthally by ±10 degrees from the symmetric position. The sequence of spherical sections obtained in this way was then stacked together in the reciprocal space, and finally the $q_y = 0$ section was built. A section built in this way is shown in Figure 2e and is much easier to interpret than the single GISAXS patterns of the same series. Moreover, it contains all the intensity related to the Fourier transform of the object shape.

The simultaneous presence of the arc and the nearest neighbor streaks is further supported by qualitative modeling performed using the IsGISAXS [34] software (Figure 2c). The parameters used in the model were as follows: stripe width 4.8 nm, stripe height 3.3 nm, stripe length 2300 nm, stripe spacing 10.5 nm. In Figure 2f–h, we present q_{xz} maps compiled from GISAXS rotation sequences measured in samples grown at 800 °C, 620 °C and 440 °C. For the sample with larger stripes, the pattern is dominated by facet streaks that correspond to the ridge confinement by {111} planes on both sides. In the sample with smaller stripes, the facet streaks are less pronounced but still present. In the sample with very small stripes grown at 440 °C, the facet streaks are totally missing. Unlike RHEED, GISAXS gathers scattering not only from the surface of the stripes but also from their volume. The most pronounced facet streaks thus appear in the large stripes for which the surface-to-volume ratio is higher. Interestingly, besides the facet streaks, the GISAXS patterns contain also the nearest neighbor streaks, seen as two vertical lines located to the left/right of the origin (Figure 2g,h). The streak separation is inversely proportional to the nearest neighbor distance in the stripe array. The most pronounced nearest neighbor streaks are observed in the sample with the small stripes. For the medium-sized stripes, these streaks are still present closer to the origin. For the large stripes, the correlation streaks are not observed, likely because they are hidden behind the beamstop. Moreover, the absence or low intensity of the nearest neighbor streaks would mean a rather weak correlation in the stripe-to-stripe distance. For the same reason, the second- and higher-

order correlation streaks are not observed. Similar GISAXS patterns have been observed in our recent publication related to Co(110) [27] and Ni(110) [8] islands grown on the CaF_2 surface. An important difference is that the metal islands were not extending micron-long in the [1–10] direction and showed additional streaks from the end facets when the X-ray beam was aligned perpendicular to the stripes.
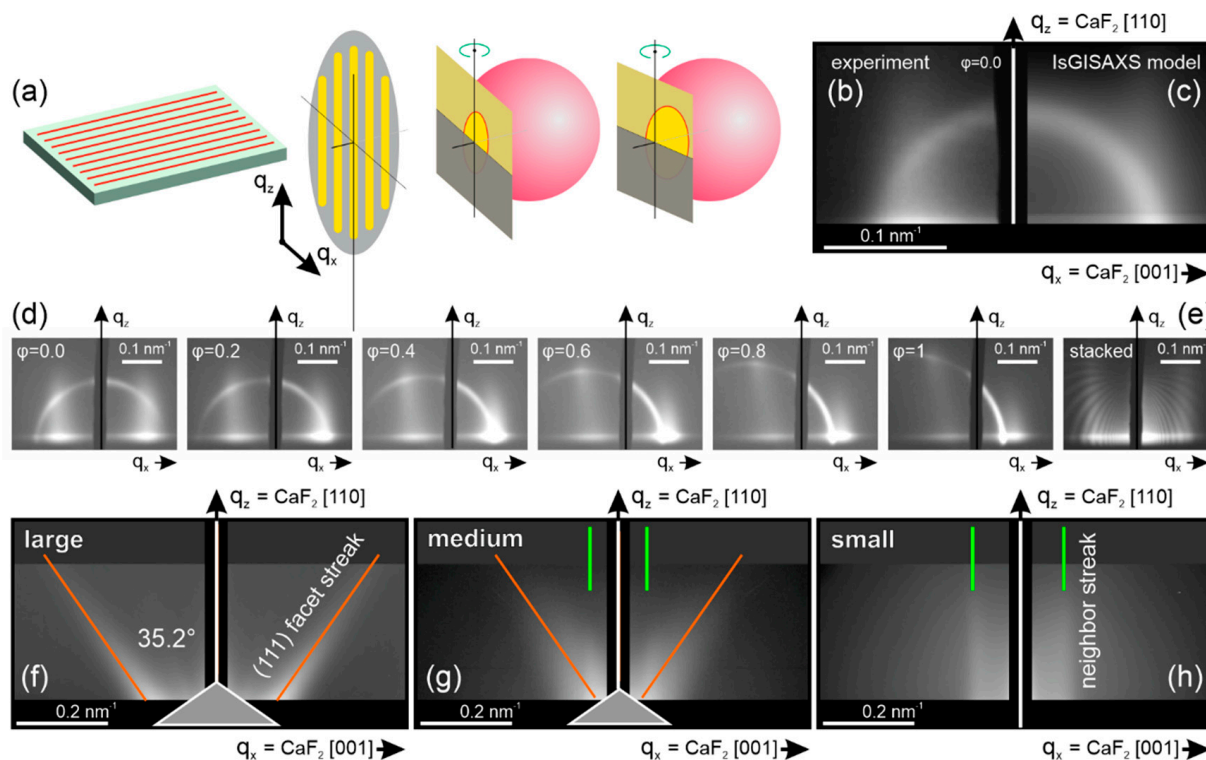

Figure 2. The reciprocal space structure corresponding to a set of parallel stripes is a flat modulated disk, whereas the arc in grazing-incidence small-angle X-ray scattering (GISAXS) results from the intersection of this disk with the Ewald sphere (**a**). The shape and position of the arc are sharply dependent on the X-ray beam azimuth with respect to the ridges (**d**). The arc+stripes GISAXS shape is confirmed by comparing experimental GISAXS pattern (**b**) with the IsGISAXS model (**c**). To reconstruct the full reciprocal space structure, one has to stack together multiple GISAXS images obtained upon sample rotation (**e**). GISAXS stacked maps obtained for CaF_2 stripes of large (**f**), medium (**g**) and small (**h**) size in the geometry where the X-ray beam travels along the ridge top. Remarkably, the inclined facet streaks become less pronounced in small ridges. On the contrary, the nearest neighbor vertical streaks become well defined in the sample with small ridges. Axis q_z is perpendicular to the substrate surface, and axis q_x is perpendicular to the stripes.

In addition to GISAXS measurements that describe scattering in the vicinity of reciprocal space origin, we also measured scattering around the CaF_2 111 off-specular Bragg reflection. This reflection was chosen as it is the brightest in CaF_2 and does not intersect with Si reflections, making it possible to accurately record the low-intensity diffuse scattering. Similarly to GISAXS maps discussed above, the intensity distribution around the CaF_2 111 reciprocal space node was reconstructed from a stack of 2D diffraction images obtained during sample rotation. The maps shown in Figure 3 represent projections of reciprocal space along the CaF2[1–10] direction parallel to the stripes. Similarly to GISAXS maps, the XRD maps show pronounced streaks perpendicular to the {111} side planes of the ridges. The facet streaks are most pronounced in large ridges, where the ratio between the facet area and the ridge volume is maximal. The contribution of the facets to X-ray scattering becomes lower as the ridges get smaller in size; in the sample with the smallest stripes, the facet streaks are indistinguishable. In addition to the {111} streaks, the maps show very well-pronounced (110) streaks that are oriented perpendicular to the surface. Due to the non-trivial epitaxial relation between Si(001) and CaF_2(110), the off-specular

crystal truncation rods of the substrate and the layer do not coincide. In particular, there is no contribution from any silicon crystal truncation rod into the CaF$_2$(111) node. This makes it possible to claim that the vertical streaks in Figure 3 are the crystal truncation rods from the flat bottoms of the CaF$_2$ stripes. As seen in Figure 3c, the sample with small ridges also shows two well-defined nearest neighbor streaks to the left/right of the main reflection. The presence of the correlation streaks around the CaF$_2$ Bragg reflection is in agreement with the earlier-presented GISAXS observation and allows the nearest neighbors to finally be identified as CaF$_2$(110) stripes.
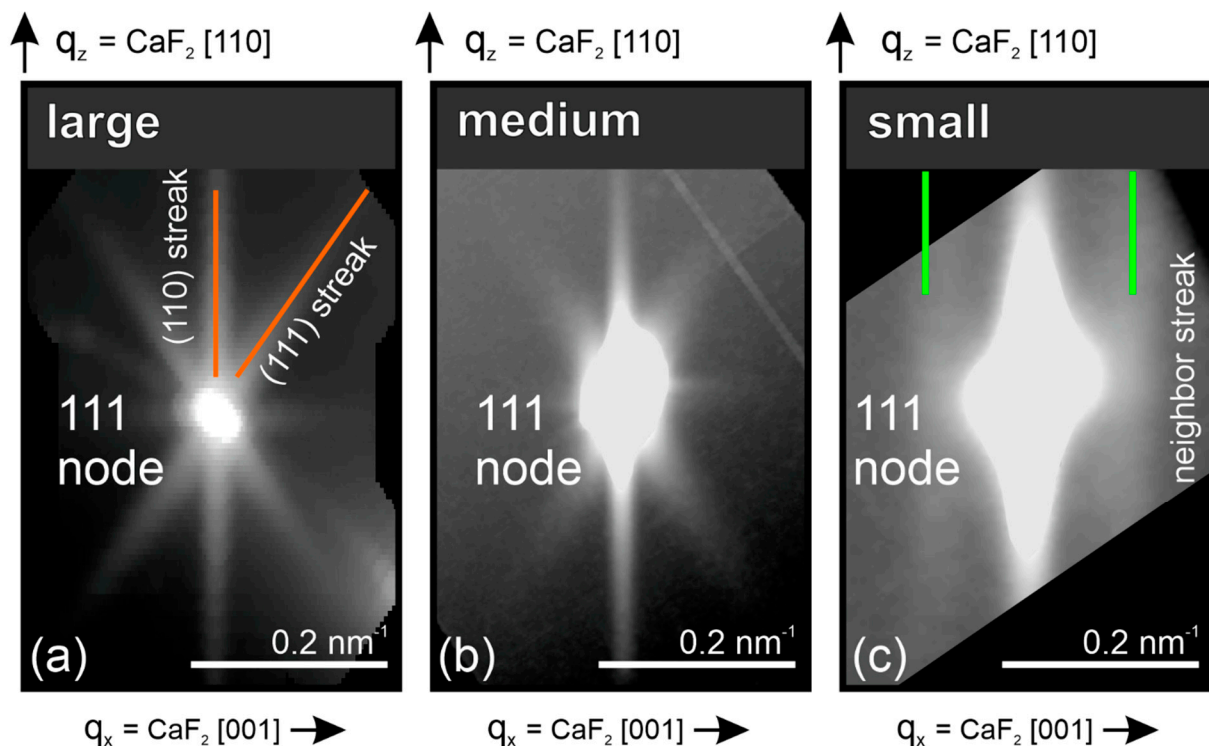

Figure 3. XRD maps obtained in CaF$_2$/Si(001) samples with large (**a**), medium (**b**) and small (**c**) stripes. The maps represent projections of reciprocal space around the CaF$_2$(111) off-specular reflection along the CaF$_2$[1–10] direction parallel to the stripes. The diffuse scattering shows pronounced streaking corresponding to the {111} side and (110) bottom facet. The facet streaks get less pronounced as the stripes become smaller. Also present on the sample with small stripes are vertical nearest neighbor streaks. Axis q$_z$ is perpendicular to the substrate surface, and axis q$_x$ is perpendicular to the stripes.

4. Conclusions

Self-assembled epitaxial CaF$_2$(110) gratings with controlled geometrical parameters have been fabricated on Si(001). The present work describes the way of controlling the dimensions of the array of fluorite stripes by choosing the substrate temperature at the second growth stage. Unlike previous publications related to CaF$_2$(110) ridges on Si(001), this work describes the array of stripes from the point of view of reciprocal space structure. By involving 3D reciprocal space mapping techniques utilizing in situ electron diffraction, ex-situ X-ray diffraction and grazing incidence small-angle scattering, we have shown the existence of non-trivial diffuse scattering around both Bragg reflections and the reciprocal space origin. This diffuse scattering in the form of {111} and (110) facet streaks as well as of (110) nearest neighbor streaks allows characterization of the array of the CaF$_2$(110) stripes from the point of view of their averaged shape and distribution. The described 3D reciprocal space mapping approach, which is unified across electron and X-ray scattering techniques, was shown to be indispensable for the study of 1D objects that, in the approach of single pattern diffraction technique, would give very limited and scarce information about the shape and nearest neighbor correlations. The fluorite gratings described in the

present paper can be utilized as natural templates, e.g., for aligning arrays of magnetic nanoparticles or large organic molecules.

References

1. Tromp, R.M.; Reuter, M.C. Structure of the Si(111)-CaF$_2$ Interface. *Phys. Rev. Lett.* **1988**, *61*, 1756–1759. [CrossRef] [PubMed]
2. Zegenhagen, J.; Patel, J.R. CaF$_2$/Si heteroepitaxy: Importance of stoichiometry, interface bonding, and lattice mismatch. *Phys. Rev. B* **1990**, *41*, 5315–5318. [CrossRef] [PubMed]
3. Rieger, D.; Himpsel, F.J.; Karlsson, U.O.; McFeely, F.R.; Morar, J.F.; Yarmoff, J.A. Electronic structure of the CaF$_2$/Si(111) interface. *Phys. Rev. B* **1986**, *34*, 7295–7306. [CrossRef] [PubMed]
4. Sugiyama, M.; Oshima, M. MBE growth of fluorides. *Microelectron. J.* **1996**, *27*, 361–382. [CrossRef]
5. Schowalter, L.J.; Fathauer, R.W. Growth and characterization of single crystal insulators on silicon. *Crit. Rev. Solid State Mater. Sci.* **1989**, *15*, 367–421. [CrossRef]
6. Sokolov, N.S.; Suturin, S.M.; Krichevtsov, B.B.; Dubrovskii, V.G.; Gastev, S.V.; Sibirev, N.V.; Baranov, D.A.; Fedorov, V.V.; Sitnikova, A.A.; Nashchekin, A.V.; et al. Cobalt epitaxial nanoparticles on CaF$_2$/Si(111): Growth process, morphology, crystal structure, and magnetic properties. *Phys. Rev. B* **2013**, *87*, 125407. [CrossRef]
7. Baranov, D.A.; Krichevtsov, B.B.; Gastev, S.V.; Banschikov, A.G.; Fedorov, V.V.; Koshmak, K.V.; Suturin, S.M.; Sokolov, N.S. Magnetic anisotropy of cobalt nanoparticle 2D arrays grown on corrugated MnF$_2$(110) and CaF$_2$(110) surfaces. *Appl. Surf. Sci.* **2013**, *267*, 196–199. [CrossRef]
8. Suturin, S.M.; Fedorov, V.V.; Korovin, A.M.; Sokolov, N.S.; Nashchekin, A.V.; Tabuchi, M. Epitaxial Ni nanoparticles on CaF$_2$ (001), (110) and (111) surfaces studied by three-dimensional RHEED, GIXD and GISAXS reciprocal-space mapping techniques. *J. Appl. Crystallogr.* **2017**, *50*, 830–839. [CrossRef]
9. Suturin, S.M.; Korovin, A.M.; Fedorov, V.V.; Valkovsky, G.A.; Tabuchi, M.; Sokolov, N.S. An advanced three-dimensional RHEED mapping approach to the diffraction study of Co/MnF$_2$/CaF$_2$/Si(001) epitaxial heterostructures. *J. Appl. Crystallogr.* **2016**, *49*, 1532–1543. [CrossRef]
10. Suturin, S.M.; Fedorov, V.V.; Banshchikov, A.G.; Baranov, D.A.; Koshmak, K.V.; Torelli, P.; Fujii, J.; Panaccione, G.; Amemiya, K.; Sakamaki, M.; et al. Proximity effects and exchange bias in Co/MnF$_2$(111) heterostructures studied by X-ray magnetic circular dichroism. *J. Phys. Condens. Matter* **2013**, *25*, 046002. [CrossRef]
11. Banshchikov, A.G.; Golosovskii, I.V.; Krupin, A.V.; Koshmak, K.V.; Sokolov, N.S.; Chernenkov, Y.P.; Yagovkina, M.A.; Ulin, V.P.; Tabuchi, M. Epitaxial layers of nickel fluoride on Si(111): Growth and stabilization of the orthorhombic phase. *Phys. Solid State* **2015**, *57*, 1647–1652. [CrossRef]
12. Rothman, A.; Dubrovskii, V.G.; Joselevich, E. Kinetics and mechanism of planar nanowire growth. *Proc. Natl. Acad. Sci. USA* **2020**, *117*, 152–160. [CrossRef]
13. Weiss, N.O.; Duan, X. A guide for nanowire growth. *Proc. Natl. Acad. Sci. USA* **2013**, *110*, 15171–15172. [CrossRef]
14. Ito, K.; Nakano, H.; Nakamura, Y. Formation of Silicon Quantum Dots Sheet on a Nonmetallic CaF$_2$ Surface. *Adv. Mater. Interfaces* **2020**, *7*, 2001295. [CrossRef]
15. Illarionov, Y.Y.; Vexler, M.I.; Fedorov, V.V.; Suturin, S.M.; Sokolov, N.S. Electrical and optical characterization of Au/CaF$_2$/p-Si(111) tunnel-injection diodes. *J. Appl. Phys.* **2014**, *115*, 223706. [CrossRef]
16. Vexler, M.I.; Sokolov, N.S.; Suturin, S.M.; Banshchikov, A.G.; Tyaginov, S.E.; Grasser, T. Electrical characterization and modeling of the Au/CaF$_2$/nSi(111) structures with high-quality tunnel-thin fluoride layer. *J. Appl. Phys.* **2009**, *105*, 083716. [CrossRef]
17. Illarionov, Y.Y.; Banshchikov, A.G.; Polyushkin, D.K.; Wachter, S.; Knobloch, T.; Thesberg, M.; Mennel, L.; Paur, M.; Stöger-Pollach, M.; Steiger-Thirsfeld, A.; et al. Ultrathin calcium fluoride insulators for two-dimensional field-effect transistors. *Nat. Electron.* **2019**, *2*, 230–235. [CrossRef]

18. Sumiya, T.; Miura, T.; Fujinuma, H.; Tanaka, S. Surface reconstruction in CaF$_2$/Si(001) investigated by scanning tunneling microscopy. *Surf. Sci.* **1997**, *376*, 192–204. [CrossRef]

19. Loretto, D.; Ross, F.M.; Lucas, C.A. Quasi-one-dimensional CaF$_2$ islands formed on Si(001) by molecular beam epitaxy. *Appl. Phys. Lett.* **1996**, *68*, 2363–2365. [CrossRef]

20. Pasquali, L.; D'Addato, S.; Selvaggi, G.; Nannarone, S.; Sokolov, N.S.; Suturin, S.M.; Zogg, H. Formation of CaF$_2$ nanostructures on Si(001). *Nanotechnology* **2001**, *12*, 403–408. [CrossRef]

21. Sokolov, N.; Suturin, S.; Ulin, V.; Pasquali, L.; Selvaggi, G.; Nannarone, S. Initial stages of MBE growth and formation of CaF$_2$/Si(001) high-temperature interface. *Appl. Surf. Sci.* **2004**, *234*, 480–486. [CrossRef]

22. Pasquali, L.; Suturin, S.; Ulin, V.; Sokolov, N.; Selvaggi, G.; Giglia, A.; Mahne, N.; Pedio, M.; Nannarone, S. Calcium fluoride on Si(001): Adsorption mechanisms and epitaxial growth modes. *Phys. Rev. B* **2005**, *72*, 045448. [CrossRef]

23. Suturin, S.M.; Sokolov, N.S.; Roy, J.; Zegenhagen, J. STM and LEED studies of CaF$_2$ submonolayer coverage on Si(001). *Surf. Sci.* **2011**, *605*, 153–157. [CrossRef]

24. Suturin, S.M.; Sokolov, N.S.; Banshchikov, A.G.; Kyutt, R.N.; Sakata, O.; Shimura, T.; Harada, J.; Tabuchi, M.; Takeda, Y. Initial Stages of High-Temperature CaF$_2$/Si(001) Epitaxial Growth Studied by Surface X-Ray Diffraction. *J. Nanosci. Nanotechnol.* **2011**, *11*, 2990–2996. [CrossRef] [PubMed]

25. Alzahrani, A.Z.; Usanmaz, D. Progressive changes in surface structure and electronic properties on Si(001) surface by CaF$_2$ adsorption. *J. Appl. Phys.* **2011**, *109*, 123708. [CrossRef]

26. Baskurt, M.; Kang, J.; Sahin, H. Octahedrally coordinated single layered CaF$_2$: Robust insulating behaviour. *Phys. Chem. Chem. Phys.* **2020**, *22*, 2949–2954. [CrossRef]

27. Suturin, S.M.; Fedorov, V.V.; Korovin, A.M.; Valkovskiy, G.A.; Konnikov, S.G.; Tabuchi, M.; Sokolov, N.S. A look inside epitaxial cobalt-on-fluorite nanoparticles with three-dimensional reciprocal space mapping using GIXD, RHEED and GISAXS. *J. Appl. Crystallogr.* **2013**, *46*, 874–881. [CrossRef]

28. Chiaravalloti, F.; Dujardin, G.; Riedel, D. Atomic scale control of hexaphenyl molecules manipulation along functionalized ultra-thin insulating layer on the Si(100) surface at low temperature (9 K). *J. Phys. Condens. Matter* **2015**, *27*, 054006. [CrossRef]

29. Duverger, E.; Boyer, A.-G.; Sauriat-Dorizon, H.; Sonnet, P.; Stephan, R.; Hanf, M.-C.; Riedel, D. Two-Dimensional Functional-ized Ultrathin Semi-Insulating CaF$_2$ Layer on the Si(100) Surface at a Low Temperature for Molecular Electronic Decoupling. *ACS Appl. Mater. Interfaces* **2020**, *12*. [CrossRef]

30. Ramos, P.; Mankarious, M.; Pavanello, M.; Riedel, D. Probing charge transfer dynamics in a single iron tetraphenylporphyrin dyad adsorbed on an insulating surface. *Nanoscale* **2018**, *10*, 17603–17616. [CrossRef]

31. Ishizaka, A.; Shiraki, Y. Low Temperature Surface Cleaning of Silicon and Its Application to Silicon MBE. *J. Electrochem. Soc.* **1986**, *133*, 666–671. [CrossRef]

32. Rueda, D.R.; Martín-Fabiani, I.; Soccio, M.; Alayo, N.; Pérez-Murano, F.; Rebollar, E.; García-Gutiérrez, M.C.; Castillejo, M.; Ezquerra, T.A. Grazing-incidence small-angle X-ray scattering of soft and hard nanofabricated gratings. *J. Appl. Crystallogr.* **2012**, *45*, 1038–1045. [CrossRef]

33. Wernecke, J.; Scholze, F.; Krumrey, M. Direct structural characterisation of line gratings with grazing incidence small-angle x-ray scattering. *Rev. Sci. Instrum.* **2012**, *83*, 103906. [CrossRef] [PubMed]

34. Lazzari, R. IsGISAXS: A program for grazing-incidence small-angle X-ray scattering analysis of supported islands. *J. Appl. Crystallogr.* **2002**, *35*, 406–421. [CrossRef]